metals

MDPI

Article

Effects of Alloying Elements on the Dissolution and Precipitation Behaviour of Fe in Mg-Al Alloy Melts

Shiyu Jiang [1,†], Li Yang [1,†], Yuan Yuan [1,2,3,*], Ligang Zhang [2], Jun Wang [1], Tao Chen [1], Aitao Tang [1], Lifeng Ma [4] and Fusheng Pan [1,3]

[1] National Engineering Research Center for Magnesium Alloys, College of Materials Science and Engineering, Chongqing University, Chongqing 400044, China; 202009131215@cqu.edu.cn (S.J.); 201709131158@cqu.edu.cn (L.Y.); wj11@cqu.edu.cn (J.W.); ct2017@cqu.edu.cn (T.C.); tat@cqu.edu.cn (A.T.); fspan@cqu.edu.cn (F.P.)
[2] School of Materials Science and Engineering, Central South University, Changsha 410083, China; ligangzhang@csu.edu.cn
[3] International Joint Laboratory for Light Alloys (Ministry of Education), Chongqing University, Chongqing 400044, China
[4] Heavy Machinery Engineering Research Center of the Ministry Education, Taiyuan University of Science and Technology, Taiyuan 030024, China; 2019001@tyust.edu.cn
* Correspondence: yuanyuan17@cqu.edu.cn or yuan.yuan.er@gmail.com
† These authors contributed equally to this work.

Abstract: It is necessary to strictly control the iron (Fe) impurity in Mg-Al alloys to guarantee good corrosion resistance and mechanical properties. In this work, the effects of alloying elements and temperatures on the solubilities of Fe in the Mg-Al-based alloy melts (Mg-rich liquid phases) at 963–1033 K were studied by combining the in situ sampling method for the high precision solution values and the multiple regression numerical analysis method for the feature analysis. The solubilities of Fe in Mg-*x*Al (x = 1 and 3 wt.%) alloy melts could be significantly reduced by adding the yttrium (Y) or manganese (Mn) elements. However, the solubilities of Fe in Mg alloy melts were not in a monotonous relationship with the contents of the alloying elements in the Mg alloys. For the addition of Mn or Y, the lowest solubilities of Fe presented in the Mg-rich liquid phases were for the Mg-*x*Al alloys with the addition of 2 wt.% Mn or 1 wt.% Y, respectively. Additionally, the Fe-containing precipitations in the related systems were analysed and the Fe was mainly combined with Mn or Y and precipitated, which contributed to the removal of Fe from the Mg melt. The present study provides fundamental thermodynamic information regarding Mg-Al-Fe based systems and the design principle for the removal of Fe in Mg alloys.

Keywords: Mg alloys; thermodynamics; liquid phase; purification

Citation: Jiang, S.; Yang, L.; Yuan, Y.; Zhang, L.; Wang, J.; Chen, T.; Tang, A.; Ma, L.; Pan, F. Effects of Alloying Elements on the Dissolution and Precipitation Behaviour of Fe in Mg-Al Alloy Melts. *Metals* **2023**, *13*, 1466. https://doi.org/10.3390/met13081466

Academic Editor: Jan Vrestal

Received: 12 July 2023
Revised: 9 August 2023
Accepted: 12 August 2023
Published: 15 August 2023

1. Introduction

As one of the lightest structural metal materials, magnesium (Mg) alloys show promise in applications in the field of aeronautics and astronautics, transport, electronic 3C, biomedical, and energy storage [1–12]. However, the corrosion properties of Mg alloys are poor due to the high chemical activity of Mg and the loose magnesium oxide film that is formed on the surface [13–36]. Different from stainless steel, the naturally formed surface oxide layers on Mg alloys are loose and porous, which cannot protect the alloy matrix from further corrosion or oxidation. Additionally, the magnesium matrix with a low standard electrode potential is prone to galvanic corrosion when combined with the presence of high electrode potential second phases [21–24]. Extensive studies have shown that impurity elements can significantly deteriorate the performance of magnesium alloys, including the corrosion-resistance performance, mechanical properties, and other required properties. It has been reported that a series of noble elements, such as iron (Fe), nickel (Ni), silicon (Si), and copper (Cu), can significantly reduce the corrosion resistance of Mg alloys [19],

where Fe impurity is the most important factor [21–24]. Additionally, the presence of the Fe element can also deteriorate the mechanical properties of Mg alloys [28].

Because of the high activity of Mg, the normal oxide crucibles are not proper for the Mg alloy synthesis. According to the phase diagram of Mg-Fe, where Fe has quite a small solubility in Mg liquid phase (around hundred ppm), as well as the low-cost and easy manufacture of Fe crucibles, Fe crucibles are broadly employed for commercial mass production of Mg alloys. As Fe crucibles have been used for dozens of years for the Mg alloy synthesizing process, a high cost will be required for replacement of the current producing systems for the commercial process. However, with the increased requirements regarding the quality of raw materials, the effects of impurities in the alloys have attracted increasing attention. As shown in our previous study, elements Fe, Ni, and Cr can all be dissolved in Mg melts and then remain in the alloys [32]. Our previous study successfully resulted in the Ni in the Mg material being below 5 ppm using a directional solidification purification method [25]. As Fe impurities are inevitably incorporated into the Mg alloys during the commercial melting and casting process, the Fe solution in the Mg alloys and the effects from Fe on the properties of Mg alloys have been studied for a long time [18–22]. Based on the current available synthesizing process, many micro-alloying methods have been proposed and have been proven to be successful strategies for Fe removal in Mg alloys [29–33].

For the corrosion of Mg alloys, the Fe-containing phases are strong cathodes coupling with the surrounding Mg matrix anodes, leading to a high micro-galvanic corrosion rate. It has been reported that Fe impurity can be transferred into some less noble second phases, such as the Al_8Mn_5 phase, and then be less active for the galvanic corrosion. Through this process, galvanic corrosion can be significantly reduced [34,35]. It has been experimentally observed that there is a tolerance limit for the content of Fe in the Mg alloys, and the corrosion rate can be rapidly increased if the content of Fe is higher than the tolerance limit, where it is later found the theoretical description of the tolerance limit is the thermodynamic equilibrium critical point for the Fe situated in the proper phases [33]. Especially, the detailed tolerance values of impurity Fe in the Mg-Al based alloys are important for the Al-containing Mg-based system, because the presence of Al will combine RE or Zr to form compounds and counteract the purification effects of Rare-earth elements and Zr [18,21].

Hence, this work focusses on the behaviour of the Fe solution in Mg-Al-based alloys. It has been reported that there is a critical weight ratio of Fe tolerance limit vs. Mn content that varies between 0.010 and 0.032 depending on the type of Mg alloy, which is cited widely in the ASTM standard [37–39]. If the ratio of Fe content vs. Mn content is higher than the critical value, the corrosion rate of the Mg alloy will sharply increase. In addition, Y is also considered as an effective alloying element for Fe removal [40–44]. Kim et al. [45] studied the removal of Fe from Mg melt through the reaction between Y and Fe, while the solution behaviour of Fe was not reported. Our previous work clearly clarified the inherit thermodynamic theory for this relationship [22,33]. In addition, Fe solubilities in the binary Mg-based systems were also studied in our group to explore the minimum solution values of Fe content in the related alloys within the thermodynamic aspect [22].

As mentioned above, the presence of Al will counteract the effects of the alloying elements in the Al-containing Mg-based system. Hence, it is important to clarify the solution and precipitation behaviour of Fe in Mg-Al-based alloy systems. The commonly employed elements, Mn and Y, are considered in this work. The study investigates the dissolution and precipitation behaviour of Fe in Mg-Al alloy melts with varied contents of micro-alloying elements and temperatures to provide basic information regarding the thermodynamics of Fe in Mg-based melts and to derive design principles for high purity Mg alloys. In our previous work [22], the addition of Al contents of 1, 3, 6, and 9 wt.% were studied for the Fe solution behaviour in Mg-Al alloys, and the first two compositions were selected for the consecutive study of the ternary system for this work. As this work aims to search for a possible microalloying method for the removal of Fe from the Mg-Al-based

alloys, the addition of small amounts of alloying elements, from 1~3 wt.%, are selected. To understand the composition-dependent behaviour, three compositions with increment of 1 wt.%, namely, 1, 2, and 3 wt.%, for each series of alloys are selected. For the studied systems, the selected compositions of the alloys are located in liquid-rich regions for the studied temperature according to the currently available thermodynamic information. The semi in situ sampling method developed by our group is used to determine the content of Fe in the melts with a high precision in real time, and the multiple regression numerical analysis method is employed to discover the thermodynamic mechanism and features.

2. Experimental Method

2.1. Materials Preparation

Pure Mg (99.99 wt.%), Pure Al (99.99 wt.%), and intermediate Mg alloys (Mg-30 wt.% Y alloy and Mg-15 wt.% Mn alloy) were used for the synthesis of alloys. Because of the high activity of Mg, the melting and isothermal treatment of Mg alloys were performed in a resistance furnace under a protective atmosphere of 0.5 vol% SF_6 and 99.5 vol% CO_2. Series alloys with different compositions (Mg-1Al-xMn (x = 0, 0.5, 2, and 3 wt.%), Mg-3Al-xMn (x = 0, 0.5, 2, and 3 wt.%), Mg-1Al-xY (x = 0, 0.5, 1, 2, and 3 wt.%), and Mg-3Al-xY (x = 0, 0.5, 1, 2, and 3 wt.%)) were melted and held in iron crucibles at 963 K, 998 K, and 1033 K. For the Mg-1Al-xMn alloy, the alloy was named Mg-1Al-1Mn (wt.%) when x = 1 wt%, and the names of the other alloys were similar. The crucibles had a depth of 250 mm and an internal diameter of 55 mm, and the thickness of 2 mm ensured a long holding time for the melt at a high temperature. The composition of the crucible employed is shown in Table 1. Then, Mg alloy melts with different alloy contents were held at 963 K, 998 K, and 1033 K, respectively, for 12 h (the temperature error is ±2 K), and the semi in situ sampling method was adopted as shown in Figure 1. As shown in our previous work [22], the Fe solution in the Mg melt approached a stable state after a holding period of 12 h. Hence, 12 h was selected for the holding time in this study. During the holding process, a small amount of melt (about 3–10 mL) was taken from the middle part of the alloy melt using an Fe tube (purity 99.9%, with inner diameter 10 mm) and it then quenched in cold water immediately. After sampling, the Fe crucibles with the remaining Mg alloy melts were quenched in cold water for further characterization. For better differentiation, the alloy solidified in the crucible was referred to as the remaining Mg alloy in this work.

Table 1. The employed chemical composition of the Fe crucible used in this work (wt.%).

Fe	C	Si	Mn	Cr	Cu	Ni	P
Bal.	<0.025	<0.0947	<0.24	<0.0204	<0.0317	<0.0091	<0.0118

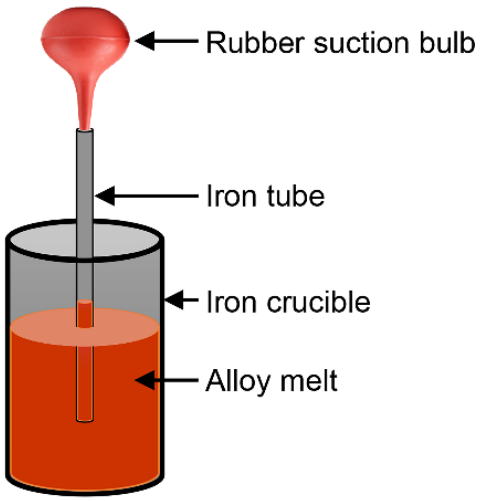

Figure 1. Schematic diagram of the sampling.

2.2. Characterization Method

Different samples were taken out from the Fe tubes for composition analysis and corrosion experiments.

All of the alloys for taken out from the Fe tubes using the semi in situ sampling method with varied studied compositions and temperatures were selected for the composition analysis. The samples were polished with SiC sandpaper and ultrasonically cleaned in ethyl alcohol to remove the surface oxides and impurities. Using the inductively coupled plasma with optical emission spectrometry (ICP-OES, Optima 8000, Agilent Ltd., Santa Clara, CA, USA), the contents of Fe in the Mg-*x*Al-X (*x* = 1 and 3 wt.%, and X = Y and Mn) melts were measured.

To further study the effects of alloying elements on the corrosion performance of Mg alloys, corrosion analysis was performed using the immersion method of plug-in specimens in the 3.5 wt.% NaCl solution saturated with Mg $(OH)_2$ at room temperature (293 K), where the hydrogen evolution volume values and weight loss values were measured. For the weight loss measurement, the corrosion products were moved by ultrasonic oscillation in the solution of 20% CrO_3 + 1% $AgNO_3$ for 5 min. For the corrosion performance analysis, the alloys taken out from the Fe tubes at 963 K were selected. They were cut into cubes of 4 × 4 × 4 mm and polished to obtain a flat surface and then ultrasonically cleaned before testing.

The hydrogen evolution rate P_H (mm·y^{-1}) and the weight loss rate P_W (mm·y^{-1}) were calculated using the immersion time t (day) and the hydrogen evolution V_H (mL cm^{-2}) as follows:

$$P_H = 2.088V_H/t \quad (1)$$

$$P_W = 2.1(W_1 - W_2)/At \quad (2)$$

where A (cm^{-2}) is the surface area. W_1 (mg) and W_2 (mg) are the dry weight of the sample before and after the immersion test, respectively.

To clarify the precipitation behaviour of the alloys during the melting status, metallographic characterization of the quenching alloys was performed. The samples were taken from the bottom of the ingots. Their dimensions were 10 × 10 × 5 mm^3 and the compositions of the second phase and precipitated particles were analysed using a field-emission scanning electron microscope (JEOL, JSM 7800F, JEOL Ltd., Hachioji, Japan) equipped with energy-dispersive X-ray spectroscopy (EDS).

3. Results and Discussion

3.1. Comparison of Fe Dissolution Pattern in Mg-xAl-X (X = Mn and Y) Ternary Alloy Melts

The Fe solubilities of Mg-*x*Al-Mn and Mg-*x*Al-Y (*x* = 1 and 3 wt.%) ternary alloys at different temperatures were obtained and are shown in Figure 2. The green dashed lines show the Fe solubility in the binary Mg-*x*Al system. With the addition of the second alloying elements, Mn and Y, the solubility values of Fe in the related ternary systems were changed, as shown in Figure 2 with different markers. The yellow dashed boxes in the figure show the minimum Fe solubility in the Mg-*x*Al-X ternary alloy at the studied temperatures. The detailed composition results are shown in Table 2. Here, the Al content is the nominal composition. As the added Al could be completely dissolved in the Mg alloy and there would be no great loss of the Al, a detailed analysis of the Al content was not performed in this work. It should be noted here the dissolved Fe amount in the melt was mainly related to the temperature and the composition of the whole alloy, not the in situ content of the alloying element, as there were precipitates that formed and settled. Hence, the nominal compositions were used for the resulting descriptions.

Table 2. The composition of the in situ sampled Mg alloys.

Nominal Alloy Compositions (wt.%)	Holding Temperature (K)	Mn or Y Content (wt.%)	Fe Content (wt.%)
Mg-1Al-0.5Mn		0.3951	0.0052
Mg-1Al-1Mn	963	0.8325	0.0026
Mg-1Al-2Mn		1.8152	0.0023
Mg-1Al-0.5Mn		0.4016	0.0151
Mg-1Al-1Mn	998	0.8613	0.0038
Mg-1Al-2Mn		1.8327	0.0043
Mg-1Al-0.5Mn		0.4108	0.0271
Mg-1Al-1Mn	1033	0.8699	0.0067
Mg-1Al-2Mn		1.8665	0.0061
Mg-3Al-0.5Mn		0.3907	0.0117
Mg-3Al-1Mn	963	0.8006	0.0054
Mg-3Al-2Mn		1.7005	0.0022
Mg-3Al-0.5Mn		0.4042	0.0265
Mg-3Al-1Mn	998	0.8102	0.0098
Mg-3Al-2Mn		1.7056	0.0052
Mg-3Al-0.5Mn		0.4099	0.0266
Mg-3Al-1Mn	1033	0.8257	0.0220
Mg-3Al-2Mn		1.7167	0.0119
Mg-1Al-0.5Y		0.4485	0.0045
Mg-1Al-1Y	963	0.7352	0.0031
Mg-1Al-2Y		1.6692	0.0035
Mg-1Al-0.5Y		0.4499	0.0086
Mg-1Al-1Y	998	0.7931	0.0071
Mg-1Al-2Y		1.6863	0.0103
Mg-1Al-0.5Y		0.4636	0.0137
Mg-1Al-1Y	1033	0.8461	0.0121
Mg-1Al-2Y		1.7041	0.0130
Mg-3Al-0.5Y		0.4011	0.0111
Mg-3Al-1Y	963	0.8779	0.0056
Mg-3Al-2Y		1.8581	0.0067
Mg-3Al-0.5Y		0.4121	0.0122
Mg-3Al-1Y	998	0.8764	0.0112
Mg-3Al-2Y		1.8933	0.0136
Mg-3Al-0.5Y		0.4124	0.0188
Mg-3Al-1Y	1033	0.8898	0.0166
Mg-3Al-2Y		1.9062	0.0173

In the studied binary and ternary alloy melts, the Fe solubilities in alloys with 1 wt.% Al were overall smaller than those in the alloys with 3 wt.% Al. In other words, the solubility values of Fe in the alloys with smaller Al contents were smaller than those in the alloys with higher Al contents. At 963 K, in the studied alloys, the smallest values for Fe solubility were 0.0022 wt.% in the Mg-3Al-2Mn alloy and 0.0023 wt.% in the Mg-1Al-2Mn alloy, respectively.

Compared with the binary Mg-Al alloy, the addition of Mn and Y could both reduce the Fe solubility values in the alloys. Among them, the Fe solubility values were generally smaller for the alloy melts with the addition of Mn elements, which indicates that the Mn element had a better effect on the removal of Fe from Mg-Al-based alloys than the Y element.

Additionally, the Fe solubility in the binary or ternary alloy melt increased significantly with the increasing temperature. The minimum solubility values of Fe in the Mg-1Al-2Mn alloy at 963, 998, and 1033 K were 0.0023, 0.0043, and 0.0061 wt.%, respectively. Hence, the low temperature casting process could generally receive the higher purity Mg alloy, where the remaining undissolved Fe was precipitated and settled to the bottom.

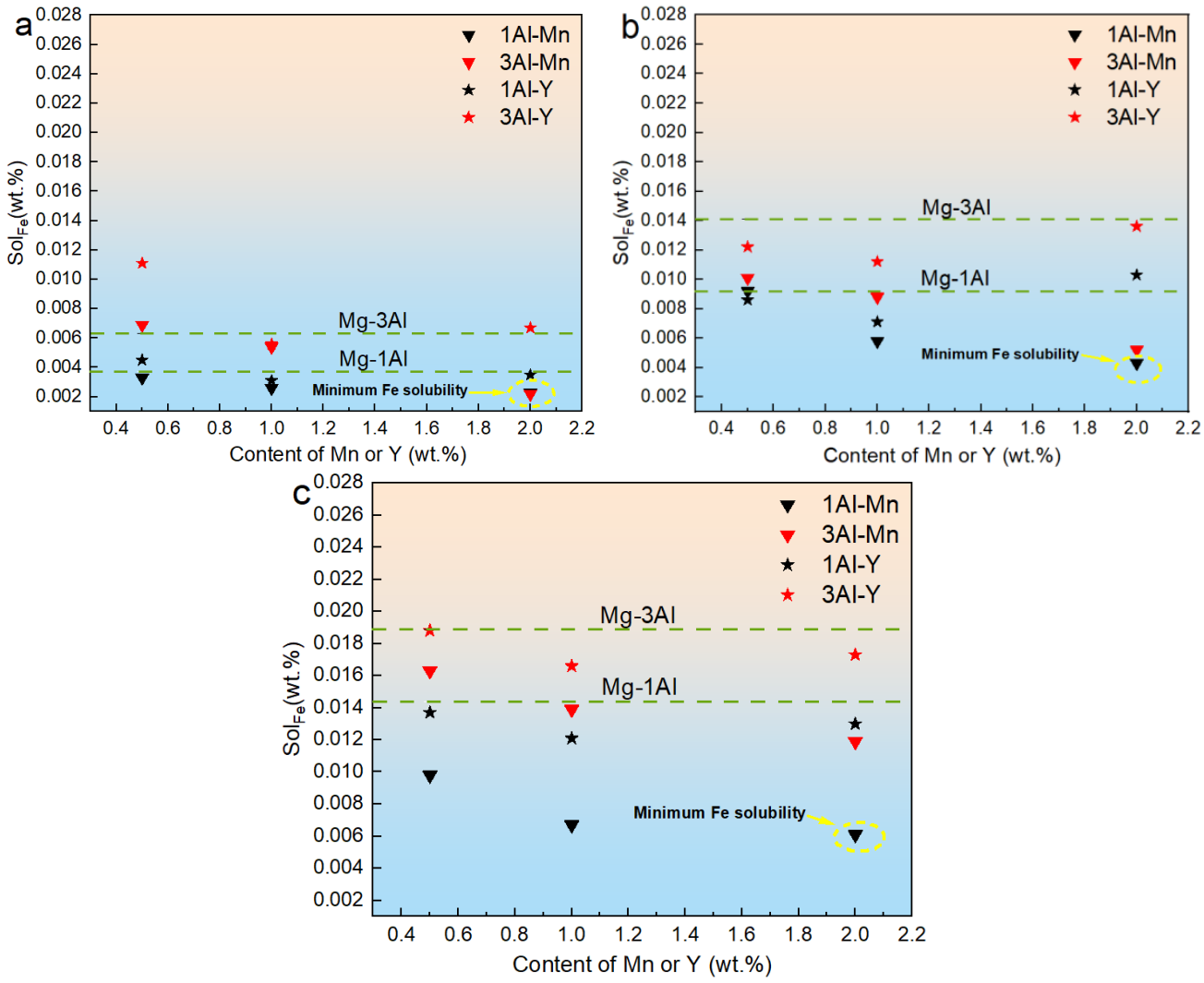

Figure 2. Solubility of Fe in the Mg-xAl-X melt at (**a**) 963 K, (**b**) at 998 K, and (**c**) at 1033 K.

3.2. Precipitation Behavior of Fe in the Melt of Mg-3Al-X Alloy

Here, this work focuses mainly on the Fe solubility in the liquid phase region to clarify the experimental thermodynamic equilibrium amount of Fe in Mg alloys. The remaining undissolved Fe will form compounds with other elements as precipitates and will settle to the low part of the region due to gravity. To clarify the solution and precipitation behaviour of Fe, Scanning Electron Microscope characterization including EDS analysis was performed to study the precipitate compounds in the bottom part of the ingots, where EDS analysis was used to for combining the elements with Fe in the precipitates. It is noted that the received precipitates may not be the theoretical equilibrium second phases in the studied temperature as the gravity effect is quite large for this type of system where the densities of components are quite different. In addition, the studied alloys are located in the Mg-rich region, where the amount and sizes of the obtained precipitates are quite small. Hence, further analysis methods are not performed. To observe the precipitates, alloys with higher alloying element contents were selected. Therefore, in this work, the precipitations of the remaining Mg-3 wt.% Al alloys were selected to study the effects of alloying elements on the precipitation and settling behaviour of Fe in the Mg-Al-based alloys, as shown in Figures 3 and 4.

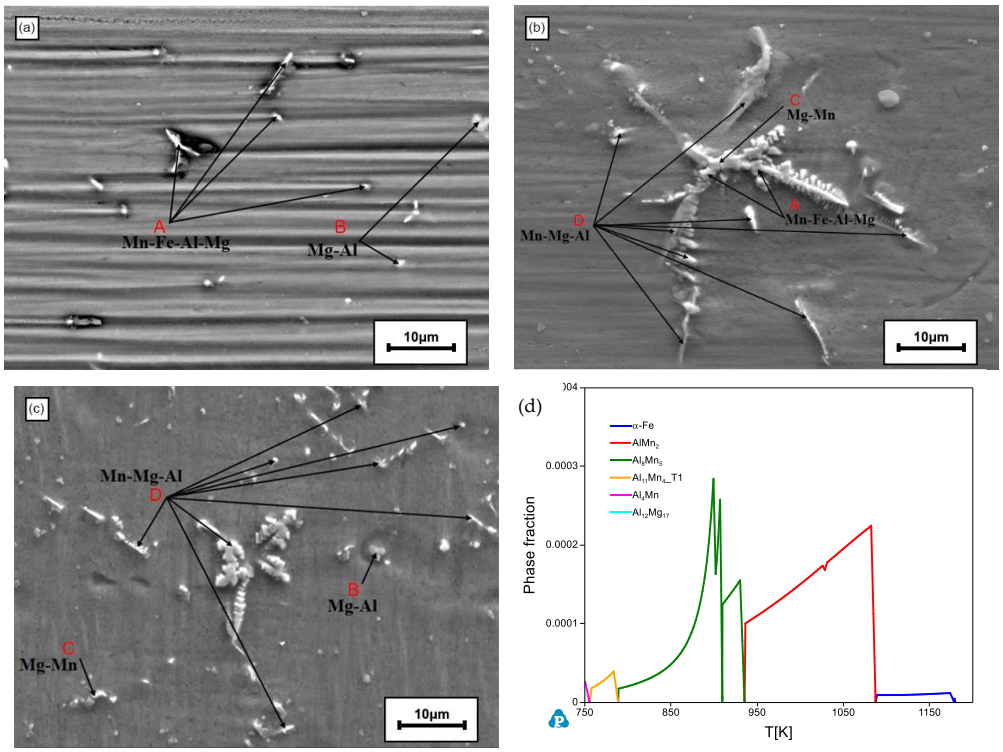

Figure 3. SEM images of the three alloys: (**a**) Mg-3Al-0.5Mn (wt.%) under BSE mode, (**b**) Mg-3Al-Mn (wt.%) under SE mode, (**c**) Mg-3Al-2Mn (wt.%) under SE mode, and (**d**) the intermediate phase fractions of Mg-3Al-2Mn-0.02Fe alloy by Scheil solidification modelling using the PanMg2023 database (the P in the image is the marker of CompuTherm LLC.).

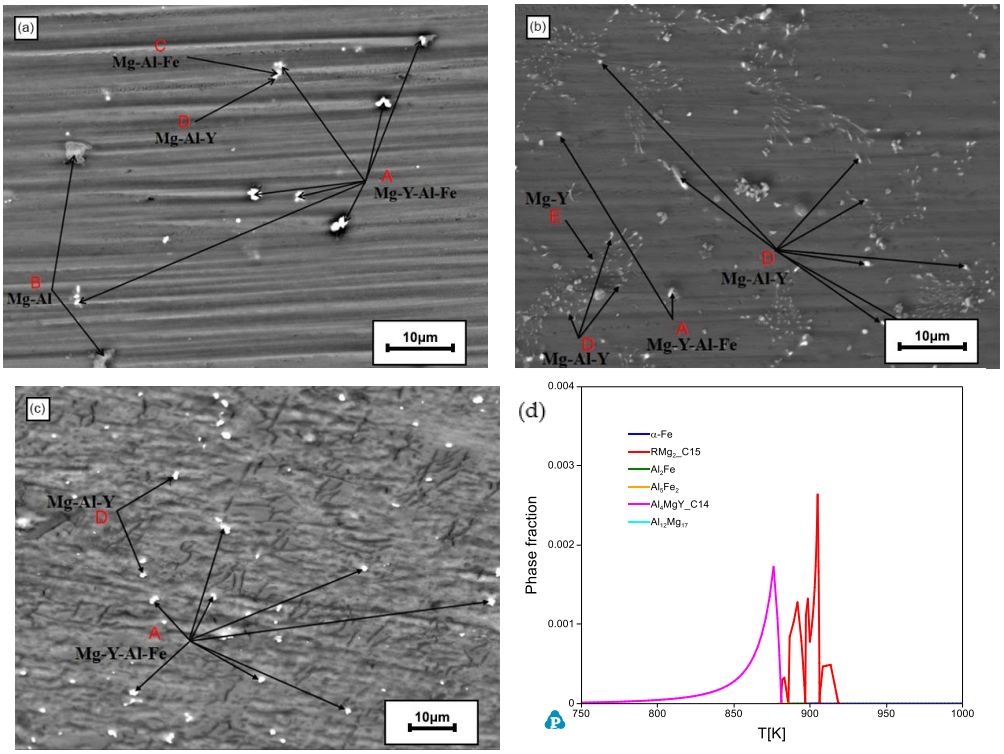

Figure 4. SEM images of the three alloys; (**a**) Mg-3Al-0.5Y (wt.%) under BSE mode, (**b**) Mg-3Al-1Y (wt.%) under SE mode, (**c**) Mg-3Al-2Y (wt.%) under BSE mode, and (**d**) the intermediate phase fractions of Mg-3Al-2Y-0.02Fe alloy by Scheil solidification modelling using the PanMg2023 database.

3.2.1. Precipitation Behaviour of Fe in the Melt of Mg-3Al-Mn Alloy

Figure 3 shows the SEM images of the bottom part of the remaining Mg-3Al-xMn (x = 0.5, 1 and 2 wt.%) alloys, and it is shown there are many compounds precipitated with different compositions. For clarity, images using different modes are presented.

Because of the small size of the precipitation particles, the detailed compositions could not be accurately measured, and so only the detected main components were labelled. The main precipitates were compounds of Mg-Al-Mn-Fe, Mg-Al, Mg-Mn, and Mg-Al-Mn. The quaternary compounds containing Mg, Al, Mn, and Fe were found at the bottom of the Mg-3Al-xMn alloys. Among these quaternary compounds, the detailed compositions showed some differences according to the EDS analysis. It was observed that the formed Fe-containing precipitates were generally larger and settled to the bottom of the crucible, which could reduce Fe solubility in the alloy melt. In addition, there was a large amount precipitation present in the Mg-Al-Mn alloys containing a higher Mn content, which may have contributed to the decreased Fe solution in the alloy melt part. As the content of Fe was below 200 ppm in the studied alloy, the distribution of Fe in the solidified phases could hardly be characterized. Hence, we used the thermodynamic calculation for the predication. The possible intermediate phases were predicted using the latest thermodynamic database of PanMg2023 and an alloy Mg-3Al-2Mn with 200 ppm Fe is taken as an example for the calculation. The Scheil solidification process (no diffusion in the solid phases) of the Mg-3Al-2Mn-0.02Fe alloy was calculated and the presented intermediate phases are shown in Figure 3d (the main phases liquid and α-Mg are not presented in the graph). It should be noted that as the thermodynamic information of the Mg-Al-Mn-Fe quaternary system was quite limited, the accuracy and precision of the current calculation using the available thermodynamic database should also be quite limited and there would also likely be some unreported intermediate phases. The calculation results show the alloys were mainly composed of Al-Mn compounds and the amount of pure Fe was quite limited. Additionally, it was reported there might be some Fe substituted in the Al-Mn phases [33]. Hence, combining the experimental results and the calculated results, it is proposed that for the Mg-Al-Mn system, Fe was mainly combined with Mn and precipitated.

According to the obtained solubilities of Fe in Mg-Al-X alloys, it has been shown that an increase in Al content will increase the solubility of Fe in the Mg-rich liquid phase. When combining the analysis of the precipitations in the alloys, it is proposed that the Mn and Al containing precipitations decrease the available amount of Mn so as to combine with Fe atoms. The non-monotonic relationship between the solubility of Fe and the content of the alloying element also shows the importance of the current study and the inherited complex thermodynamic behaviour. However, because of the lack of information about the compounds and thermodynamics of the quaternary Mg-Al-Mn-Fe system, the thermodynamic assessment of the whole system was not performed in this work.

3.2.2. Precipitation Behavior of Fe in the Melt of Mg-3Al-Y Alloy

Figure 4 shows the SEM images of the bottom of the remaining Mg-3Al-xY (x = 0.5, 1 and 2 wt.%) alloys. The main precipitates were compounds of Mg-Y-Al-Fe, Mg-Al, Mg-Y, Mg-Al-Fe, and Mg-Al-Y. Similar to the Mg-Mn-Al alloy, the low Y content in the melt was due to the settled precipitates containing Fe and Y, which was consistent with the ICP results. The precipitates in the alloys with higher Y contents showed a bigger size. The Scheil solidification process of the Mg-3Al-2Y-0.02Fe alloy was calculated and the presented intermediate phases are shown in Figure 4d (the main phases of liquid and α-Mg are not presented in the graph). According to the calculation predication, the amount of α-Fe was much less than that in the Mg-3Al-2Mn-0.02Fe alloy and there were some Al-Fe compounds presented. The calculated results show, for the Mg-Al-Y system, the Fe was mainly combined with Al. According to our previous study [2], the elements with similar features were more likely to be substituted by each other. Different to the Mg-Al-Mn-Fe system, Fe was likely not able to substitute Y in the Y-containing intermediate phase as Fe and Y were quite different atomically. Hence, combining the experimental results and the

calculation analysis, it is proposed that there are probably some quaternary phases in the Mg-Al-Y-Fe system and more extensive study on this system is needed; however, this was out of the scope of this work.

3.3. Effects of Micro-Alloying on the Corrosion Performance of Mg-Al Alloys

The results of hydrogen evolution on Mg-Al binary alloys, Mg-Al-Mn ternary alloys, and Mg-Al-Y ternary alloys are shown in Figures 5a, 6a and 7a, respectively. The hydrogen evolution and weight loss rates for these binary and ternary alloys are shown in Figures 5b, 6b and 7b, respectively. For these experiments, two parallel samples were prepared and the general error range of the result was within 10%. The obtained values with different periods for each alloy followed quite a good parabolic rule, which indicates that the obtained values were reliable.

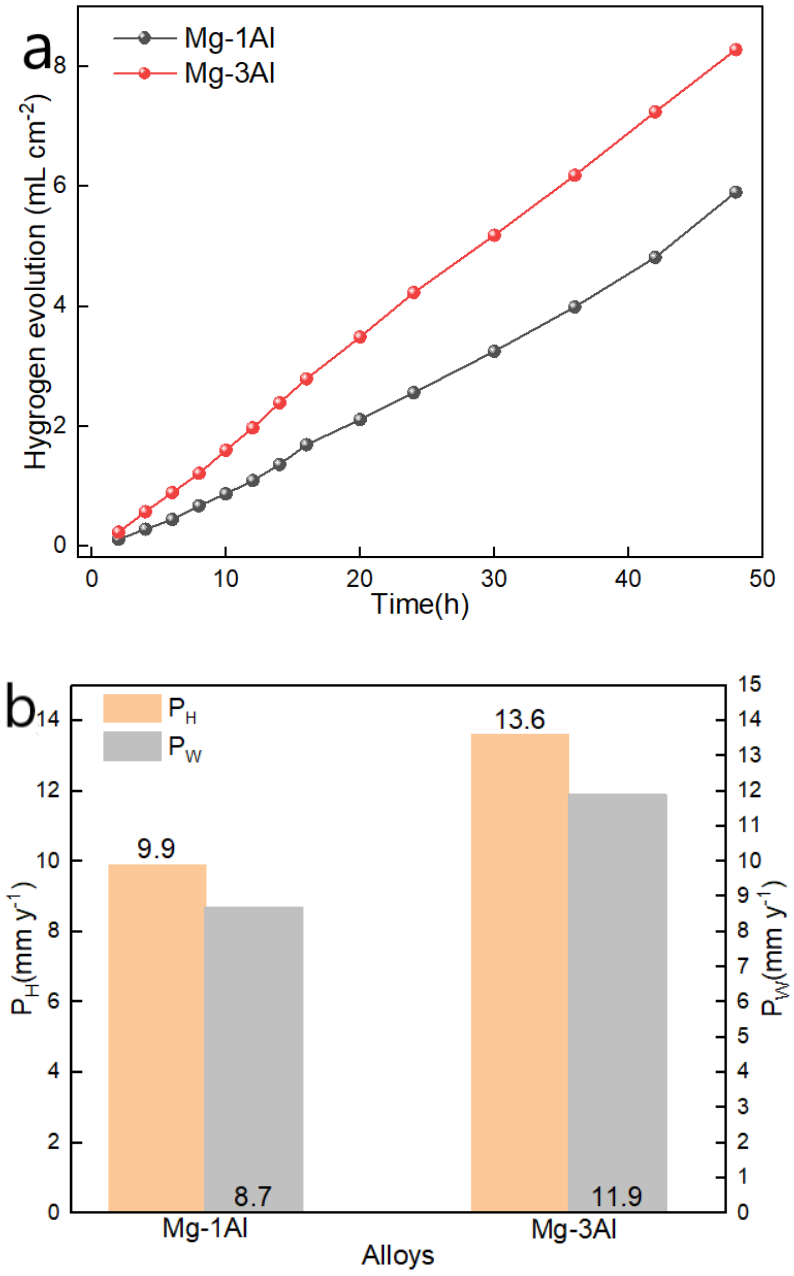

Figure 5. (**a**) Hydrogen evolution and (**b**) hydrogen evolution and weight loss rate of Mg-1 wt.% Al and Mg-3 wt.% Al alloys after soaking in 35 (±1) g/L NaCl solution at 293 K (±2) at room temperature for 48 h.

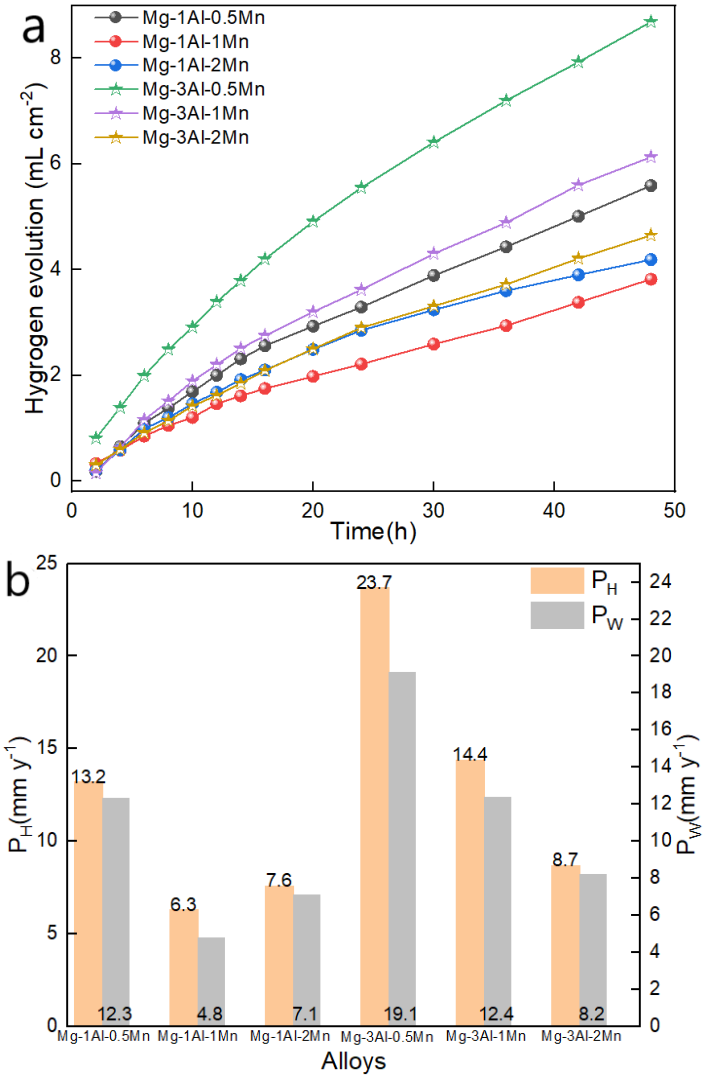

Figure 6. (**a**) Hydrogen evolution and (**b**) hydrogen evolution and weight loss rate of the Mg-1,3Al-xMn (wt.%) alloy after soaking in 35 (±1) g/L NaCl solution at 293 K (±2) at room temperature for 48 h.

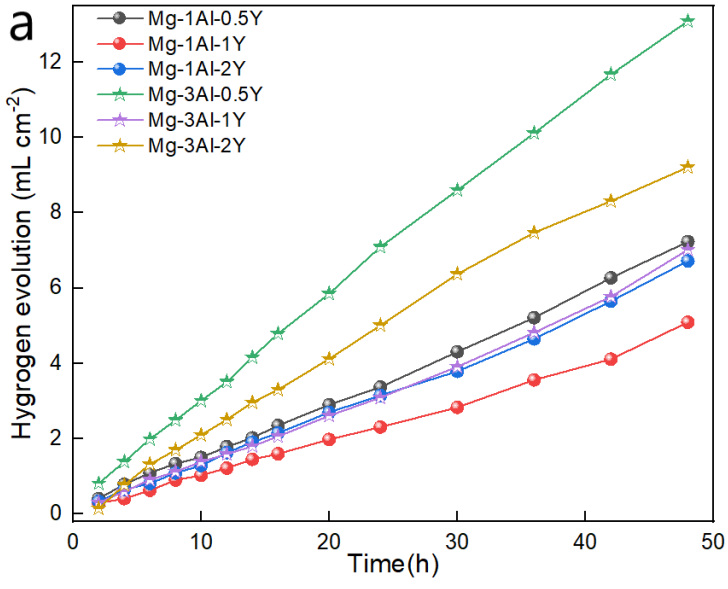

Figure 7. *Cont*.

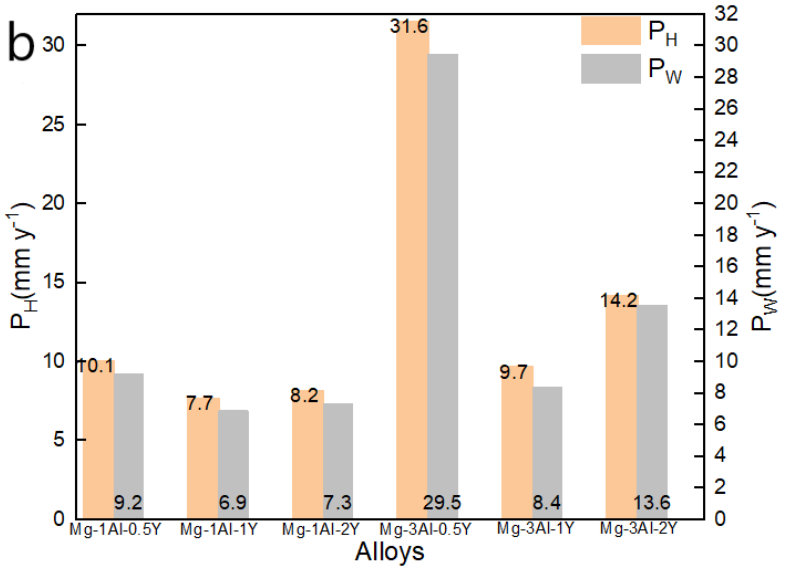

Figure 7. (**a**) Hydrogen evolution and (**b**) hydrogen evolution and weight loss rate of the Mg-1, 3Al-*x*Y (wt.%) alloy after soaking in 35 (±1) g/L NaCl solution at 293 K (±2) at room temperature for 48 h.

3.3.1. Effects of Al on the Corrosion Performance of Mg Alloys

The relationships between the hydrogen evolution volume and immersion time of Mg-1Al and Mg-3Al alloys are shown in Figure 5a. The amount of hydrogen evolution increased with increasing the immersion time in a linear manner. The corrosion rates did not change much with the increase in immersion time. Figure 5b shows that the behaviour of the hydrogen evolution rate P_H was the same as that of the weight loss rate P_W. The P_H and P_W values of the Mg-1Al alloy, 9.9 and 8.7 mm·y^{-1}, respectively, were less than those of the Mg-3Al alloy. Kim et al. [45] reported that the corrosion rate of commercially pure magnesium was 230 mm·y^{-1} using the hydrogen evolution experiment in 3.5% NaCl solution for 72 h. It can be seen that the hydrogen evolution corrosion rate of Mg could be significantly reduced by adding a small amount of Al. With the increase in Al content, the hydrogen evolution and weight loss rates increased, which may be related to the higher Fe solubility in Mg alloys with higher Al contents.

3.3.2. Effects of Mn on the Corrosion Performance of Mg Alloys

Figure 6a shows the relationship between the hydrogen evolution volume and immersion time of Mg-1Al-*x*Mn and Mg-3Al-*x*Mn alloys in the NaCl solution for 48 h. The parabolic relationships for the studied Mg-Al-Mn ternary alloys are displayed between the amount of hydrogen evolution and immersion time, which shows the corrosion property of these alloys are stable in the studied period. As shown in Figure 6b, the trends of hydrogen evolution and weight loss rates for all of the studied Mg-Al-Mn ternary alloys were the same, and the overall hydrogen evolution and weight loss rate of the Mg-1Al-*x*Mn (x = 0.5, 1, and 2 wt.%) alloys were lower than those of the Mg-3Al-*x*Mn (x = 0.5, 1, and 2 wt.%) alloys. The addition of the Mn element reduced the amount of hydrogen evolution for the Mg alloys, and the Mg-1Al-1Mn alloy had the lowest hydrogen evolution rate. The further increase in Mn content would also deteriorate the corrosion performance of the Mg alloys.

The hydrogen evolution and weight loss rate of the Mg-1Al-1Mn alloys were the smallest, with values of 6.3 and 4.8 mm·y^{-1}, respectively. Combining Figures 2a and 6a, the Fe solubility in Mg-3Al-*x*Mn (x = 0.5, 1 and 2 wt.%) decreased with the increase in Mn content, and their corrosion rates also decreased gradually.

3.3.3. Effects of Y on the Corrosion Performance of Mg Alloys

From Figure 7a, it is found that linear relationships for the studied Mg-Al-Y ternary alloys were displayed between the amount of hydrogen evolution and the immersion time. It can be seen that their hydrogen evolution volumes increased with the increase in immersion time. As presented in Figure 7a, as the Y content increased, the corrosion rates of Mg-Al-Y ternary alloys with certain Al contents did not change in a linear way, where the values first decreased and then increased with a minimum point of 1 wt.% Y content. The corrosion rates of all Mg-1Al-*x*Y (x = 0.5, 1 and 2 wt.%) alloys were smaller than those of the Mg-3Al-*x*Y (x = 0.5, 1 and 2 wt.%) alloys.

With increasing the Y content in the Mg-Al-Fe alloy, the changes in Fe solubility were similar to the changes in the corrosion rates, where the Fe solubility decreased first and then increased, and the lowest Fe solubility was at point of Mn content of 1 wt.%.

Comparing Figures 5–7, it can be found that the corrosion rates decreased through the addition of Y and the effect was not as strong as that with the addition of Mn, which may be attributed to the better effect of Mn in reducing Fe solubility in the Mg alloy melt.

3.3.4. The Comparison of the Fe Solution Behaviour in the Mg-Al-Mn System and Mg-Al-Y System

In this work, the two common alloying elements were studied. Element Mn has long been reported to be able to effectively remove Fe from magnesium alloys. Our previous study on thermodynamics has validated the linear relationship between the Mn content and Fe tolerance limit, where the location phase region of the alloy is the determining factor [33]. In our studied composition region, the solubility of Fe decreased with the addition of Mn from 0 wt.% to 3 wt.% for both Mg-1Al and Mg-3Al systems. With the addition of too much Mn, the formation of large Mn-containing precipitates also deteriorated the corrosion-resistance properties of Mg alloys. As shown in the corrosion test, the Mg-1Al-1Mn alloy had the best corrosion resistance property among the studied alloys.

Comparing the two studied systems, the solubility of Fe in the Y-containing system was generally bigger than that of the Mn-containing system, and the corrosion resistance of the Y-containing alloys was also generally bigger than those of the Mn-containing alloys. Considering the cost and density of these two alloying elements, Mn is still the best active and effective element for the Fe purification of Mg alloys. The addition of Mn can reduce the Fe solution in the liquid phase as well as in the solid phase, and, additionally, Mn can further enclose the remaining Fe in the intermediate phase to reduce the bad effect coming from Fe. In our study [46,47], Mn is also the perfect low-cost element for the grain-refinement of Mg alloys. As the effective strengthening element, Y is also broadly used in Mg alloys.

It is seen that compared with the binary Mg-Al system, Fe solubility can be reduced to around 20 ppm for the addition of Mn or Y. It can be expected with a lower temperature that close to the eutectic temperature, the solubility of Fe in the liquid phase will be much lower. Hence, this work indicates that the Fe content in the Mg-Al alloys with micro-alloying Mn or Y can be theoretically be reduced to around 20 ppm, but probably not less, which can meet the normal purity requirement of Mg-Al-based alloys. If a higher purity is required for the Al-containing Mg alloys, the other methods may need to be performed.

4. Conclusions

(1) The solubility of Fe in Mg-Al alloy melts can be reduced by micro-alloying Y or Mn. Additionally, the Fe solubility in the melts is not monotonously dependent on the content of the alloying element. The lowest point of Fe solubility in the Mg-Al-Y ternary alloy melt was at 1 wt.% Y with the same Al content.

(2) There were many precipitations containing Mg, Fe, Al, and X (X = Mn or Y) settled at the bottom of the Mg alloys, which is attributed to the removal of Fe from the melt.

(3) The micro-alloying of Mn and Y of 0.5–2 wt.% can significantly reduce the hydrogen evolution corrosion rates of Mg-Al alloys as both Mn and Y elements can effectively

reduce the Fe solubility in Mg-Al alloys and also react with Fe to form less noble intermediate phases. Among the studied alloys, the Mg-1Al-1Mn alloy with the lowest Fe content showed the best corrosion resistance.

This work provides fundamental information regarding the thermodynamics of Mg-based systems and the design principles for the purification method to obtain high purity and high-performance Mg alloys.

Author Contributions: Conceptualization, Y.Y.; Methodology, S.J. and J.W.; Software, T.C. and A.T.; Validation, S.J.; Formal analysis, S.J. and L.Y.; Investigation, S.J.; Resources, L.Z., L.M. and F.P.; Data curation, T.C.; Writing—original draft, S.J. and L.Y.; Writing—review and editing, L.Y. and Y.Y.; Supervision, Y.Y.; Project administration, Y.Y. and F.P.; Funding acquisition, Y.Y. All authors have read and agreed to the published version of the manuscript.

Funding: This research was funded by the National Natural Science Foundation of China (grant numbers: 51971044, U1910213, 52171100, and U20A20234), the Scientific Research Foundation for the Returned Chinese Scholars of Chongqing Human Resources and Social Security Bureau (cx2021109). The technology support by Testing Center of Chongqing University is greatly acknowledged.

Data Availability Statement: The datasets generated during and/or analysed during the current study are available upon request.

Conflicts of Interest: The authors declare no conflict of interest.

References

1. Wang, J.; Yuan, Y.; Chen, T.; Wu, L.; Chen, X.; Jiang, B.; Wang, J.; Pan, F. Multi-solute solid solution behavior and its effect on the properties of magnesium alloys. *J. Magnes. Alloys* **2022**, *10*, 1786–1820. [CrossRef]
2. Chen, T.; Gao, Q.; Yuan, Y.; Li, T.; Xi, Q.; Liu, T.; Tang, A.; Watson, A.; Pan, F. Coupling physics in machine learning to investigate the solution behavior of binary Mg alloys. *J. Magnes. Alloys* **2022**, *10*, 2817–2832. [CrossRef]
3. Li, D.; Yuan, Y.; Liu, J.; Fichtner, M.; Pan, F. A review on current anode materials for rechargeable Mg batteries. *J. Magnes. Alloys* **2020**, *8*, 963–979. [CrossRef]
4. Huang, D.; Cao, F.; Ying, T.; Zheng, D.; Song, G.-L. High-energy-capacity metal-air battery based on a magnetron-sputtered Mg–Al anode. *J. Power Sources* **2022**, *520*, 230874. [CrossRef]
5. Fu, Q.; Liang, W.; Huang, J.; Jin, W.; Guo, B.; Li, P.; Xu, S.; Chu, P.K.; Yu, Z. Research perspective and prospective of additive manufacturing of biodegradable magnesium-based materials. *J. Magnes. Alloys* **2023**, *11*, 1485–1504. [CrossRef]
6. Wang, J.; Meng, L.; Xie, W.; Ji, C.; Wang, R.; Zhang, P.; Jin, L.; Sheng, L.; Zheng, Y. Corrosion and in vitro cytocompatibility investigation on the designed Mg-Zn-Ag metallic glasses for biomedical application. *J. Magnes. Alloys* **2022**, *10*, 1786–1820. [CrossRef]
7. Zheng, X.; Song, C.; Yuan, Y.; Li, D.; Gu, D.; Wu, L.; Huang, G.; Wang, J.; Pan, F. High stability In–Sn–Bi multi-element alloy anode for Mg ion batteries. *J. Power Sources* **2023**, *575*, 233141. [CrossRef]
8. Zhang, L.; Yuan, Y.; Wang, J.; Chen, T.; Wang, J.; Pan, F. The ultrahigh damping capacity of Mg-Sn-Y alloy. *Scr. Mater.* **2023**, *233*, 115514. [CrossRef]
9. Li, Y.; Yuan, Y.; Wang, J.; Wu, L.; Cao, F.; Zhang, L.; Pan, F. Controllable degradation behavior of Mg-Sr-Y alloys for the bio-applications. *NPJ Mater. Degrad.* **2023**, *7*, 353. [CrossRef]
10. Cai, L.; Mei, D.; Zhang, Z.-Q.; Huang, Y.-D.; Cui, L.-Y.; Guan, S.-K.; Chen, D.-C.; Kannan, M.B.; Zheng, Y.-F.; Zeng, R.-C. Advances in bioorganic molecules inspired degradation and surface modifications on Mg and its alloys. *J. Magnes. Alloys* **2022**, *10*, 670–688. [CrossRef]
11. Zhu, Q.; Li, Y.; Cao, F.; Qiu, D.; Yang, Y.; Wang, J.; Zhang, H.; Ying, T.; Ding, W.; Zeng, X. Towards development of a high-strength stainless Mg alloy with Al-assisted growth of passive film. *Nat. Commun.* **2022**, *13*, 5838. [CrossRef]
12. Dai, X.; Wu, L.; Ci, W.; Yao, W.; Yuan, Y.; Xie, Z.; Jiang, B.; Wang, J.; Andrej, A.; Pan, F. Dual self-healing effects of salicylate intercalated MgAlY-LDHs film in-situ grown on the micro-arc oxidation coating on AZ31 alloys. *Corros. Sci.* **2023**, *220*, 111285. [CrossRef]
13. Wu, L.; Yang, D.; Zhang, G.; Zhang, Z.; Zhang, S.; Tang, A.; Pan, F. Fabrication and characterization of Mg-M layered double hydroxide films on anodized magnesium alloy AZ31. *Appl. Surf. Sci.* **2018**, *431*, 177–186. [CrossRef]
14. Wu, J.; Yuan, Y.; Yu, X.; Chen, T.; Li, D.; Wu, L.; Jiang, B.; Atrens, A.; Pan, F. The high-temperature oxidation resistance properties of magnesium alloys alloyed with Gd and Ca. *J. Mater. Sci.* **2021**, *56*, 8745–8761. [CrossRef]
15. Wu, J.; Yuan, Y.; Yang, L.; Chen, T.; Li, D.; Wu, L.; Jiang, B.; Steinbrück, M.; Pan, F. The oxidation behavior of Mg-Er binary alloys at 500 °C. *Corros. Sci.* **2022**, *195*, 109961. [CrossRef]
16. Shen, G.; Lyu, S.; Yu, L.; Li, T.; You, C.; Wang, X.; Chen, M.; Jiang, B. Effect of nano-CaO particle on the microstructure, mechanical properties and corrosion behavior of lean Mg-1Zn alloy. *J. Magnes. Alloys*, 2023; *in press*. [CrossRef]

17. Zhang, G.; Wu, L.; Tang, A.T.; Ma, Y.L.; Song, G.L.; Zheng, D.J.; Jiang, B.; Atrens, A.; Pan, F.S. Active corrosion protection by a smart coating based on a MgAl-layered double hydroxide on a cerium-modified plasma electrolytic oxidation coating on Mg alloy AZ31. *Corros. Sci.* **2018**, *139*, 370–382. [CrossRef]
18. Chen, T.; Yuan, Y.; Mi, X.; Wu, J.; Tang, A.; Wang, J.; Moelans, N.; Pan, F.S. Interaction of elements in dilute Mg alloys: A DFT and machine learning study. *J. Mater. Res. Technol.* **2022**, *21*, 4512–4525. [CrossRef]
19. Esmaily, M.; Svensson, J.E.; Fajardo, S.; Birbilis, N.; Frankel, G.S.; Virtanen, S.; Arrabal, R.; Thomas, S.; Johansson, L.G. Fundamentals and advances in magnesium alloy corrosion. *Prog. Mater. Sci.* **2017**, *89*, 92–193. [CrossRef]
20. Lei, Y.; Zhan, M.; Xin, H.; Ma, L.; Yuan, Y.; Zhang, H.; Zheng, Z. Comparison of the Strain Rate Sensitivity in AZ31 and WE43 Magnesium Alloys under Different Loading Conditions. *Crystals* **2023**, *13*, 554. [CrossRef]
21. Chen, T.; Yuan, Y.; Wu, J.J.; Liu, T.T.; Chen, X.H.; Tang, A.T.; Pan, F.S. Alloy Design Strategies of the Native Anti-corrosion Magnesium Alloy. In *Magnesium Technology 2019*; Springer International Publishing: Berlin/Heidelberg, Germany, 2019; pp. 169–173.
22. Jiang, S.; Yuan, Y.; Wang, J.; Chen, T.; Wu, L.; Chen, X.; Jiang, B.; Tang, A.; Pan, F. Effect of alloying elements on the dissolution behavior of iron in magnesium melt. *Calphad* **2022**, *79*, 102503. [CrossRef]
23. Cao, F.; Xiao, B.; Wang, Z.; Ying, T.; Zheng, D.; Atrens, A.; Song, G.L. A Mg alloy with no hydrogen evolution during dissolution. *J. Magnes. Alloys* **2021**, *11*, 2084–2095. [CrossRef]
24. Zhang, C.; Wu, L.; Liu, H.; Huang, G.; Jiang, B.; Atrens, A.; Pan, F. Microstructure and corrosion behavior of Mg-Sc binary alloys in 3.5 wt.% NaCl solution. *Corros. Sci.* **2020**, *174*, 108831. [CrossRef]
25. Wang, J.; Yuan, Y.; Zhang, Y.; Feng, X.; Chen, T.; Chen, X.; Jiang, B.; Yang, Y.; Pan, F. A method of removal of nickel impurity from electrolytic magnesium. *Vacuum* **2022**, *203*, 111310. [CrossRef]
26. Liu, M.; Uggowitzer, P.J.; Nagasekhar, A.V.; Schmutz, P.; Easton, M.; Song, G.L.; Atrens, A. Calculated phase diagrams and the corrosion of die-cast Mg-Al alloys. *Corros. Sci.* **2009**, *51*, 602–619. [CrossRef]
27. Makar, G.L.; Kruger, J. Corrosion of Magnesium. *Int. Mater. Rev.* **1993**, *38*, 138–153. [CrossRef]
28. Arora, G.S.; Saxena, K.K.; Mohammed, K.A.; Prakash, C.; Dixit, S. Manufacturing Techniques for Mg-Based Metal Matrix Composite with Different Reinforcements. *Crystals* **2022**, *12*, 945. [CrossRef]
29. Gusieva, K.; Davies, C.H.J.; Scully, J.R.; Birbilis, N. Corrosion of magnesium alloys: The role of alloying. *Int. Mater. Rev.* **2015**, *60*, 169–194. [CrossRef]
30. Ha, H.Y.; Kang, J.Y.; Yang, J.; Yim, C.D.; You, B.S. Role of Sn in corrosion and passive behavior of extruded Mg-5 wt.% Sn alloy. *Corros. Sci.* **2016**, *102*, 355–362. [CrossRef]
31. Yin, H.; Chen, J.H.; Yan, H.G.; Xia, W.J.; Su, B.; Huang, W.S.; Yan, X.X. Effects of Zn Addition on Microstructure, Mechanical, and Corrosion Properties of the As-Solutionized Mg-5Ga Alloy. *J. Mater. Eng. Perform.* **2021**, *30*, 4411–4420. [CrossRef]
32. Chen, T.; Xiong, X.; Yuan, Y.; Tang, A.T.; Li, D.J.; Atrens, A.; Pan, F.S. Effect of Steels on the Purity of Molten Mg Alloys. *Adv. Eng. Mater.* **2020**, *22*, 2000338. [CrossRef]
33. Chen, T.; Yuan, Y.; Liu, T.T.; Li, D.J.; Tang, A.T.; Chen, X.H.; Schmid-Fetzer, R.; Pan, F.S. Effect of Mn Addition on Melt Purification and Fe Tolerance in Mg Alloys. *JOM* **2021**, *73*, 892–902. [CrossRef]
34. Andreatta, F.; Apachitei, I.; Kodentsov, A.A.; Dzwonczyk, J.; Duszczyk, J. Volta potential of second phase particles in extruded AZ80 magnesium alloy. *Electrochim. Acta* **2006**, *51*, 3551–3557. [CrossRef]
35. Byun, J.Y.; Kwon, S.; Ha, H.P.; Yoon, J.K. A Manufacturing Technology of AZ91-Alloy Slurry for Semi Solid Forming. In *Magnesium: Proceedings of the 6th International Conference Magnesium Alloys and Their Applications*; Wiley-VCH Verlag GmbH & Co. KGaA: Weinheim, Germany, 2005; pp. 713–718.
36. Chen, Y.; Wu, L.; Yao, W.; Wu, J.; Serdechnova, M.; Blawert, C.; Zheludkevich, M.L.; Yuan, Y.; Xie, Z.; Pan, F. "Smart" micro/nano container-based self-healing coatings on magnesium alloys: A review. *J. Magnes. Alloys* 2023, *in press*. [CrossRef]
37. Hillis, J. The Effects of Heavy Metal Contamination on Magnesium Corrosion Performance. *SAE Trans.* **1983**, *92*, 553–559. [CrossRef]
38. James, D.W.; Staack, G.C.; Hunyadi Murph, S.E. Tritium Aging of LaNi4.15Al0.85 (LANA.85). *Fusion Sci. Technol.* **2017**, *71*, 565–569. [CrossRef]
39. Luo, A.A. Magnesium casting technology for structural applications. *J. Magnes. Alloys* **2013**, *1*, 2–22. [CrossRef]
40. Liu, L.; Yuan, F.; Zhao, M.; Gao, C.; Feng, P.; Yang, Y.; Yang, S.; Shuai, C. Rare Earth Element Yttrium Modified Mg-Al-Zn Alloy: Microstructure, Degradation Properties and Hardness. *Materials* **2017**, *10*, 477. [CrossRef]
41. Chen, G.; Peng, X.D.; Fan, P.G.; Xie, W.D.; Wei, Q.Y.; Ma, H.; Yang, Y. Effects of Sr and Y on microstructure and corrosion resistance of AZ31 magnesium alloy. *Trans. Nonferr. Met. Soc. China* **2011**, *21*, 725–731. [CrossRef]
42. Matsubara, H.; Ichige, Y.; Fujita, K.; Nishiyama, H.; Hodouchi, K. Effect of impurity Fe on corrosion behavior of AM50 and AM60 magnesium alloys. *Corros. Sci.* **2013**, *66*, 203–210. [CrossRef]
43. Song, J.; She, J.; Chen, D.; Pan, F. Latest research advances on magnesium and magnesium alloys worldwide. *J. Magnes. Alloys* **2020**, *8*, 1–41. [CrossRef]
44. Li, L.; Nam, N.D. Effect of yttrium on corrosion behavior of extruded AZ61 Mg alloy. *J. Magnes. Alloys* **2016**, *4*, 44–51. [CrossRef]
45. Kim, J.I.; Nguyen, H.N.; You, B.S.; Kim, Y.M. Effect of Y addition on removal of Fe impurity from magnesium alloys. *Scr. Mater.* **2019**, *162*, 355–360. [CrossRef]

46. Liao, H.; Kim, J.; Liu, T.; Tang, A.; She, J.; Peng, P.; Pan, F. Effects of Mn addition on the microstructures, mechanical properties and work-hardening of Mg-1Sn alloy. *Mater. Sci. Eng. A* **2019**, *754*, 778–785. [CrossRef]
47. Wu, X.; Jing, X.; Xiao, H.; Ouyang, S.; Tang, A.; Peng, P.; Feng, B.; Rashad, M.; She, J.; Chen, X.; et al. Controlling grain size and texture in Mg–Zn–Mn alloys from the interaction of recrystallization and precipitation. *J. Mater. Res. Technol.* **2022**, *21*, 1395–1407. [CrossRef]